aerospace

MDPI

Article

Experimental Assessment of Aero-Propulsive Effects on a Large Turboprop Aircraft with Rear-Engine Installation

Salvatore Corcione *, Vincenzo Cusati, Danilo Ciliberti and Fabrizio Nicolosi

Department of Industrial Engineering, University of Naples "Federico II", Via Claudio 21, 80125 Naples, Italy
* Correspondence: salvatore.corcione@unina.it

Abstract: This paper deals with the estimation of propulsive effects for a three-lifting surface turboprop aircraft concept, with rear engine installation at the horizontal tail tips, conceived to carry up to 130 passengers. This work is focused on how the propulsive system affects the horizontal tailplane aerodynamics and, consequently, the aircraft's static stability characteristics using wind tunnel tests. Both direct and indirect propulsive effects have been estimated. The former produces moments whose values depend on the distance from the aircraft's centre of gravity to the thrust lines and propeller disks. The latter entails a change in the angle of attack and an increment of dynamic pressure on the tailplane. Several tests were also performed on the body-empennage configuration to investigate the propulsive effects on the aircraft's static stability without the appearance of any aerodynamic interference phenomena, especially from the canard. The output of the experimental campaign reveals a beneficial effect of the propulsive effects on the aircraft's longitudinal stability, with an increase in the stability margin of about 2.5% and a reduction in the directional stability derivative of about 4%, attributed to the different induced drag contributions of the two horizontal tail semi-planes. Moreover, the rolling moment coefficient experiences a greater variation due to the propulsion depending on the propeller rotation direction. The outcomes of this paper allow the enhancement of the technical readiness level for the considered aircraft, giving clear indications about the feasibility of the aircraft configuration.

Keywords: innovative turboprop; wind tunnel tests; three-lifting surface; experimental aerodynamics; aircraft design; propeller slipstream

Citation: Corcione, S.; Cusati, V.; Ciliberti, D.; Nicolosi, F. Experimental Assessment of Aero-Propulsive Effects on a Large Turboprop Aircraft with Rear-Engine Installation. *Aerospace* **2023**, *10*, 85. https://doi.org/10.3390/aerospace10010085

Academic Editor: Kung-Ming Chung

Received: 16 December 2022
Revised: 12 January 2023
Accepted: 13 January 2023
Published: 15 January 2023

1. Introduction

Market scenarios and environmental requirements have brought aircraft manufacturers and research institutes to investigate non-conventional, innovative configurations for more efficient transport aircraft. Remarkable examples are represented by the blended wing body layout [1,2] and the box wing [3–5] configurations. Another interesting concept is based on introducing a third lifting surface, the canard, ahead of the main conventional wing-tail arrangement, a concept known as the Three-Surface Aircraft (TSA) configuration [6–10]. The advantages and challenges of the TSA concept have been widely assessed during the last two decades. Early investigations were addressed to evaluate induced as well as viscous drag under trimmed conditions [11]. Several wind-tunnel tests have been performed to produce comparative data between the three-surface, canard-wing, and conventional tailplane configurations [12] and to provide basic aerodynamic data concerning multi-surface aircraft configurations to assess specific design features for the combination of a canard, wing, and tailplane to improve aircraft aerodynamic performance [13]. A business/commuter advanced turboprop design has been recently investigated using a wind tunnel test, demonstrating that a three-surface layout with aft-mounted engines can achieve greater longitudinal stability, a reduced wing aerodynamic drag, and up to 20% increase in centre-of-gravity range with respect to a conventional wing-tail layout [14]. Trade-off studies and canard optimisation in a three-lifting-surface transport aircraft by

means of both numerical simulations and wind tunnel tests have shown promising results in terms of fuel savings [6].

A renewed interest in the three-lifting surface configuration has been generated by a recent research project named IRON, which has assessed the feasibility study of a high-capacity turboprop aircraft [15]. The investigation of different configurations, including the TSA, showed that the three-lifting-surface layout is a design solution that could potentially help to reduce the environmental impact of regional aircraft with respect to the current state-of-the-art regional jets. The design of a large-capacity turboprop aircraft (increasing the number of passengers from 70 to 130–150) leads to heavier aircraft, with a larger wing area, increased wingspan, and, in turn, larger propellers. As shown in [15], a new turboprop aircraft configuration should be characterised by a rear-mounted engine installation, enabling an extended laminar flow region on the wing to improve the overall aerodynamic efficiency and reducing the cabin noise owing to the propulsive plant far from the passengers' cabin.

The exploitation of the aft engine installation was already explored in the early 1980s by Douglas Aircraft Company. They performed a feasibility study about the design modification of the DC-9 (with a seating capacity of 155–165 pax) with aft-mounted propellers, aiming at increasing the fuel efficiency with respect to the turbofan-powered baseline aircraft. The aft propeller installation was favourable in terms of potential fuel savings, although it was also found that further investigations were needed to demonstrate these savings along with adequate stability and handling qualities [16].

The installation of propellers on a lifting surface, such as the horizontal tailplane, results in strong aero-propulsive effects. Interactions between propellers and wings have been assessed in the case of wing-tip installation in [17], whereas the impact in terms of stability and control has been investigated in [18]. Recent works dealt with the slipstream effects that must be taken into account in the preliminary sizing of the horizontal empennage to ensure the trim capabilities of and sufficient static stability in the whole range of the centre of gravity excursion [19]. The impact the propellers have on both the longitudinal stabiliser and the elevator aerodynamics has been assessed by means of numerical and experimental wind tunnel tests, highlighting the fact that the aerodynamic interaction of the tail-tip installed propellers and the tail itself leads to a 20% variation in the tail lift curve slope and elevator effectiveness [20–22].

How can a propeller affect the aerodynamics of a lifting surface? A propeller can be defined as a rotating fluid machine capable of providing thrust to an aircraft by converting the mechanical energy from the engine into kinetic energy. Each propeller blade cross-section is an airfoil generating thrust in the same way that a wing airfoil produces lift [23]. Propellers as a whole generate thrust by changing momentum into a streamtube flowing through the propeller disk area. In this perspective, an attractive way to represent the propeller is the concept of an advancing rotating wing that produces a helical vortex system as sketched in Figure 1.

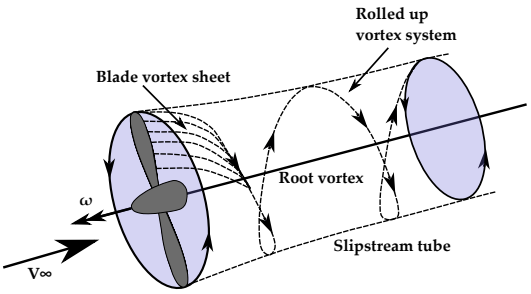

Figure 1. Vortex system and slipstream tube behind a propeller.

The vortex wake behind the propeller tends to deform and to roll up, producing the so-called slipstream tube in which there are strong gradients of several aerodynamic quantities—i.e., axial velocity and swirl velocity profiles, total and static pressure distributions, vorticity, helicity, and wake contraction. Numerical and experimental investigations

have demonstrated that the propeller-wing interaction effects, in the case of a tractor–propeller configuration, resulted in drag reduction [24–26]. This can be explained given that the propeller swirl produces regions of upwash and downwash on a lifting surface affected by the propeller slipstream. The region of the wing laying in the upwash region is affected by a local increase in the angle of attack leading to an increase in the local lift coefficient. Furthermore, the force vector is tilted forward with a positive lift and negative drag component or thrust, as sketched for section A-A of Figure 2.

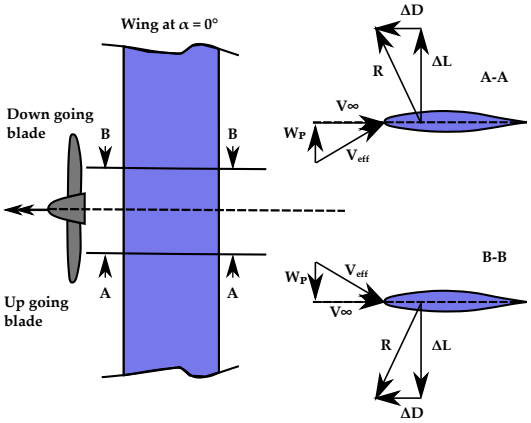

Figure 2. Local forces on a wing section inside the propeller slipstream: upwash region (section A-A) and downwash region (section B-B).

If the wing is located in the downwash region of the propeller, the local angle of attack decreases, resulting in a reduction in the local lift coefficient, and the force vector is tilted backwards, producing a negative lift component and a negative drag component, see section B-B of Figure 2. It is the so-called recover swirl, since the negative component of the drag—that is, thrust—reduces the swirl losses. Generally speaking, for finite wings, the lift loading is greater inboard than outboard, causing greater drag reductions for inboard-up rotating propellers compared to outboard-up rotating propellers. Since loading gradients are generally stronger near the wing tip, the positive effect of the propeller slipstream in terms of drag reduction will be greater when propellers are placed at the wing tip [27].

Two other effects that must be considered are the changes of axial velocity and swirl in the propeller slipstream impacting the wing aerodynamic behaviour. The lifting surface regions lying inside the propeller slipstream experience greater dynamic pressures due to the higher axial velocities. A propeller at a zero angle of attack has an axisymmetric flow field. However, the axial velocity changes in the radial direction; thus, the increase in dynamic pressure depends on the vertical position of the propeller with respect to the wing. Contrary to this, the effect of the tangential velocity in the slipstream is asymmetrical, producing an increase or a decrease in the local angles of attack depending on whether the blade is going upward or downward in front of the wing. When the aerodynamic coefficients are calculated with respect to the free stream conditions, the net result on the wing lift will be positive due to increased dynamic pressure on both sides of the propeller axis [26]. The effect of the propeller's slipstream on the wing spanwise loading is sketched in Figure 3.

In the case of rear engines installed on the horizontal tail, there are some relevant differences with respect to a conventional wing-mounted configuration. Tail-mounted propellers act on a lifting surface with a reduced aspect ratio, and the propeller diameter is relatively large compared with the tail span. Moreover, in the specific case of a tail-tip installation, a complex interaction between the tail tip-vortex and the propeller slipstream will occur. This interaction is even more complex considering that the tail is required to produce lift force in both negative and positive directions by changing the elevator deflection, which affects the tail loading distribution [20].

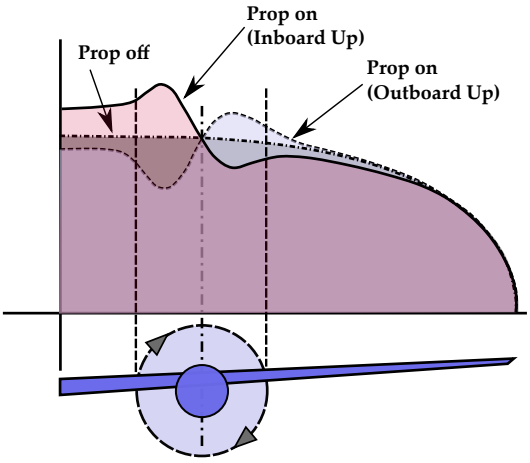

Figure 3. Effects of propeller slipstream on wing loading.

Generally speaking, the propellers installed at wing tips should be counter-rotating, inboard-up to increase the efficiency of the wing-propeller interactions [28], but commercial propeller-driven aircraft are generally provided with co-rotating propellers for cost reasons [16]. Thus, if the latter is also the case for tail-mounted propeller aircraft, the asymmetry in the loading distribution on the tailplane should be addressed.

The propeller slipstream can also affect the aircraft's directional stability and control, especially in case one engine is inoperative. In that case, an asymmetrical flow field exists on the vertical tail, receiving an increased dynamic pressure on only one of its sides. Moreover, the sidewash in the case of one engine being inoperative will be greater when the inboard-up engine is the operative one [29]. The main reason for the sideforce is the asymmetric lift distribution created over the vertical tail. The swirl and the increased axial velocity behind the propeller cause a large amount of additional lift on the side where the propeller blade moves upwards due to the local change in the angle of attack, creating a strong trailing vortex. The large asymmetric spanwise lift distribution over the wing–fuselage combination causes a greater downwash on one side of the aircraft. This increased downwash causes a circulation around the fuselage, which in turn changes the incoming flow at the vertical tail, creating a side force [23,30].

The generation of the asymmetric lift distribution for an inboard-up and outboard-up propeller and the effect on the vertical tail are sketched in Figure 4. The inboard-up rotating propeller generates a peak in lift coefficient closer to the fuselage. This causes the circulation around the fuselage to be greater. For this reason, the outboard-up engine is the critical engine: if it fails, the largest adverse yawing moment on the aircraft is generated. To compensate for it, a large rudder deflection is required. If the inboard-up engine fails, a much smaller rudder deflection is required since the crossflow caused by the slipstream of the operating engine is weaker.

In general, all the effects coming from the slipstream interaction with aircraft components are defined as indirect effects. On the contrary, direct effects are related to the aerodynamic forces exerted by and on the propeller: the thrust T and the normal force N. The latter is orthogonal to the thrust line, and it is generated in non-axial flows. As a side product, both thrust and normal force produce aerodynamic moments on the aircraft, whose values depend on the distance of the aircraft's centre of gravity to the propulsive forces lines of action. Although direct effects may be predicted with methods identified in the literature [31–33], indirect effects are of the same order of magnitude, but much more difficult to estimate.

The aim of this paper is the experimental assessment of both direct and indirect propulsive effects on the stability characteristics of the IRON three-lifting surface aircraft configuration with rear-mounted engines [15,34,35]. Notwithstanding the complexity of scaling the propeller slipstream effects, the experimental apparatus has been set up

to attempt the matching of the propeller's thrust coefficient C_T for a few representative flight conditions.

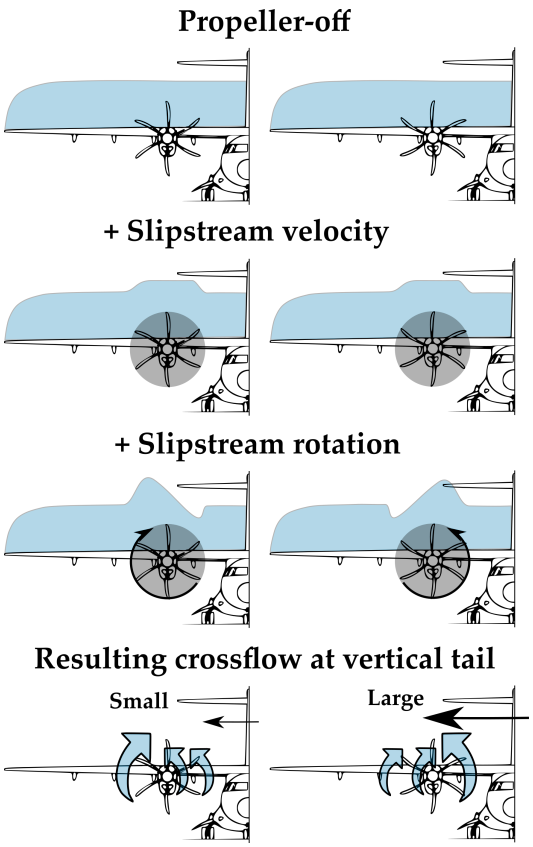

Figure 4. Effects of propeller slipstream on vertical tail due to the wing loading distributions caused by inboard-up and outboard-up rotations.

This work is focused on the prediction of the impact the propulsive system has on the horizontal tailplane aerodynamics and, consequently, the aircraft static stability characteristics in an innovative large turboprop aircraft design characterised by three-lifting surfaces. The investigation is complicated by the interference effects among aircraft components, in particular by the effects of the combined downwash coming from both canard and wing, and of their wakes on the empennage aerodynamics. Very poor data are available in the literature concerning a three-lifting surface configuration for a high-capacity passenger aircraft with and without the propulsive effects. The innovation of this work is properly intended in this direction. It provides an experimental evaluation of the aerodynamic characteristics of a three-lifting surface turboprop aircraft, including propulsive effects, and it represents an important dowel towards the demonstration of the technical feasibility of such an innovative configuration. In particular, the outcomes of this paper allow the enhancement of the technical readiness level of the considered aircraft, giving clear indications on several aspects concerning propulsive effects and their interaction with the interference effects among the lifting surfaces and their effect on aircraft stability.

The remainder of the paper is organised as follows. Section 2 describes the experimental apparatus and the propulsive system used to perform the wind tunnel test campaign. Section 3 shows the main achievements in assessing the propellers, slipstream effects on fuselage and empennage configuration. Isolated fuselage and empennage have been considered to isolate the propulsive effects, avoiding as much as possible any other interference issue coming from other aircraft components—i.e., the canard wake and vortex system. In Section 4, the impact the propellers have on the complete aircraft configuration is shown, highlighting how, in this particular three-lifting surface arrangement, the canard wake and

tip vortexes have a deep interaction with the propeller slipstream. Finally, in Section 5, some conclusions are drawn.

2. Propulsive System for Wind Tunnel Test

The design of a propulsive system for wind tunnel tests on a scaled model involves several aspects to properly reproduce the physical behaviour. To achieve thrust similarity, the propeller thrust and torque coefficients of the scaled model must be the same as the full-scale aircraft. Ideally, to achieve complete thrust similarity, both the propeller axial and tangential factors should be matched with their full-scale values. Practically, this is almost impossible, especially for the latter. In fact, propellers should be geometrically similar and operate at the same advanced ratio [36]—that is, the propeller should be investigated at full scale.

Unfortunately, in this case, the aircraft does not exist yet, and therefore, the full-scale propeller geometry is not available. Moreover, the propeller blade Reynolds number should be very close to the full-scale value, while on the scaled model, the flow speed of the wind tunnel is limited by the maximum power available to the fan or the maximum load tolerated by the strain gauge balance.

For all the above reasons, the axial and rotational flow speeds were scaled differently: the propeller advance ratio J and the thrust coefficient C_T were the same for the full-scale aircraft, whereas the torque and the power coefficients C_Q and C_P of the scaled propeller were not matched. Consequently, the swirl and the induced angle of attack distribution due to the rotation of the scaled propeller may be different from those generated by the full-scale item.

However, as the objective of the wind tunnel test campaign was the evaluation of propulsive effects on aircraft stability characteristics, it was decided to attempt to match the thrust coefficient C_T for a few representative flight conditions. Details of the propeller design are given in [37]. A drawing of the propeller's planform is given in Figure 5, whereas its characteristics measured in the wind tunnel are shown in Figure 6.

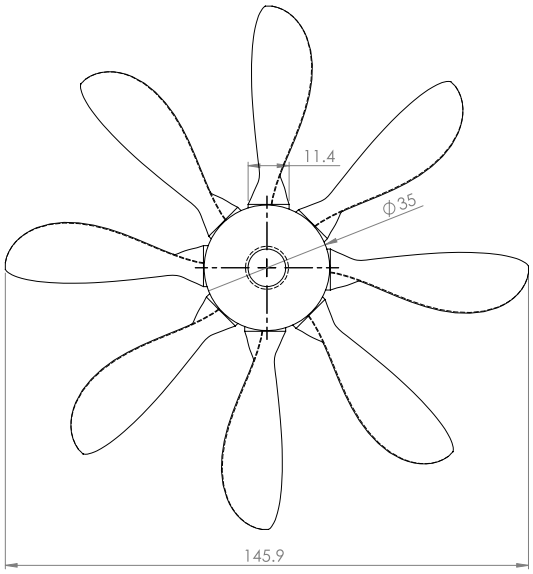

Figure 5. Planform of the propeller model for wind tunnel testings [37]. Units in mm.

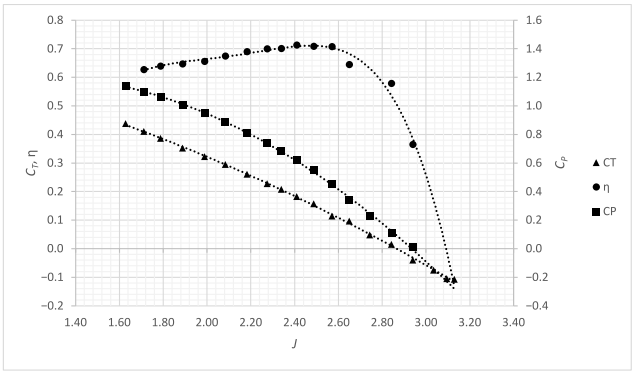

Figure 6. Isolated propeller characteristics from wind tunnel measurements [37].

Wind Tunnel Instrumentation

Some notes on the wind tunnel hardware and mechanical system used for tests are here reported. The wind tunnel model of the aeroplane was manufactured using aluminium alloy, through CNC machining. It had a scale ratio of 1:25 with a wing span of 1.50 m, a mean aerodynamic chord of about 0.13 m, and a fuselage length of about 1.52 m. Figure 7 illustrates the main geometric characteristics of the scaled model. Wind tunnel tests were performed at an average wind tunnel speed of 35 m/s, with a Reynolds number evaluated on the mean aerodynamic chord of about 315,000. To replicate the boundary layer of the full-scale aircraft, two layers of zig-zag strips were installed to promote flow transition. Specifically, strips were at 5% of the local chord for lifting surfaces (wing, horizontal and vertical tail) and on the fuselage nose at 10% of body length.

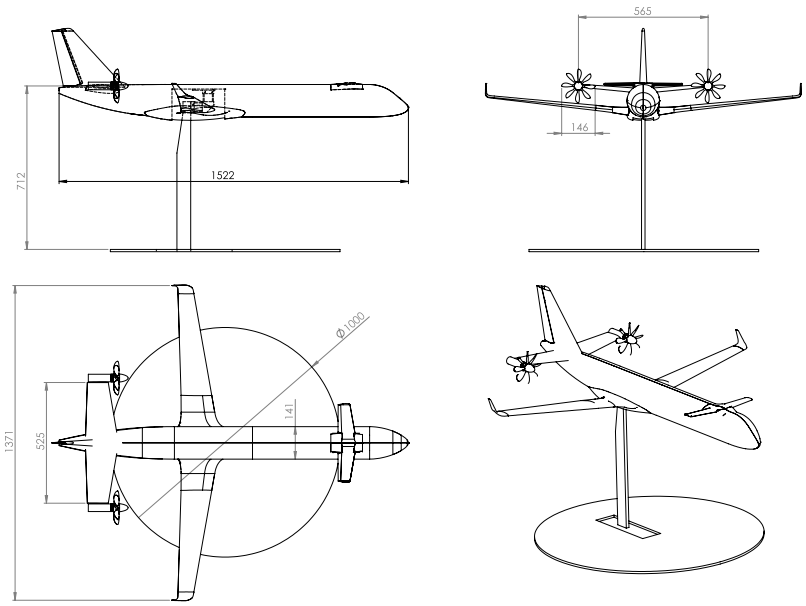

Figure 7. IRON scaled model with the main balance, motors, and propellers. Motor supporting frame not represented. Units in mm.

The scaled propulsive system was supported by a frame with a narrow box under each motor containing the Electronic Speed Controller (ESC), two orthogonal S-shaped load cells to measure propeller thrust and normal force, and a custom printed circuit board to power the sensors and provide signal conditioning.

The load cells dedicated to the motors were 10 kg full-scale with 2.0 mV/V nominal sensitivity providing a resolution of about 0.2 N. The ESC was an air-cooled MGM Compro HBC-series with 2048-bit resolution and a maximum operating voltage of 63 V. A temperature sensor and an RPM counter were installed directly on each motor case. Data acquisition and motor control were performed with a National Instruments USB-6341

board. The power supply was provided by four 12 V 54 Ah lead batteries that generated a constant voltage for a reasonable amount of time and absorbed power in the case of propeller braking. The frequency of the data acquisition and motor control system was set to 3000 Hz with a buffer of 1000 samples. This means that at 9000 RPM the system acquired 20 revolutions of the propellers while making three average measurements per second. A scheme of the system is given in Figure 8.

It was decided to separate the propulsive system from the aircraft model to avoid eventual vibrations on the main balance. However, the motors were located sufficiently close to the aircraft. The model balance measured the indirect propulsive effect, while the load cells installed on the motors' supporting frame measured propeller thrust and normal forces only. This supporting frame provided clamps for the motors as well as housing for the ESC and the load cells. The motors moved along three orthogonal axes and rotated about the local pitch axis, following the different attitudes of the aircraft. This operation was manually performed with the wind tunnel off.

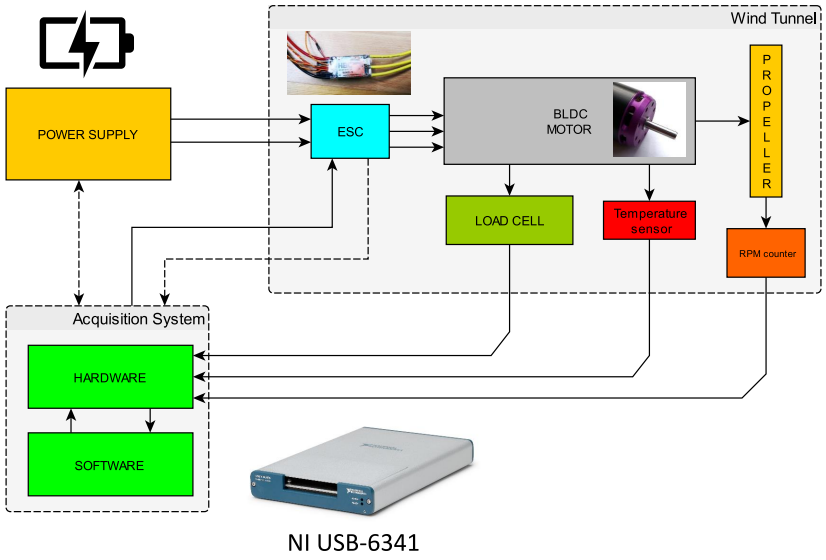

Figure 8. Scheme of the wind tunnel system for propulsive tests.

Undeniably, one of the principal characteristics of the system just described is compactness. Figure 9 illustrates the concept. It is possible to see the electronics for motor control and propulsive data acquisition, as well as the two orthogonal S-beam cells measuring thrust and normal forces.

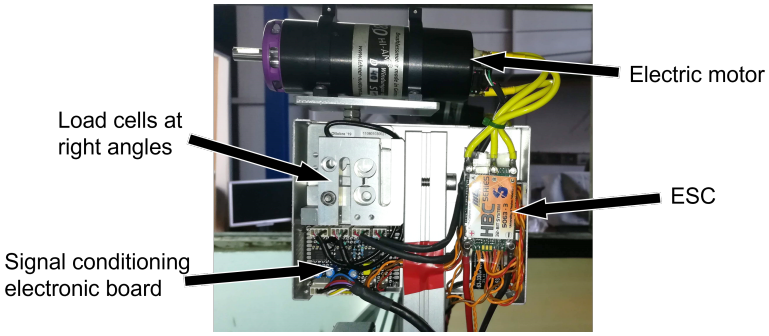

Figure 9. Details of electronics for data acquisition of the propulsive forces and signal conditioning for motor control.

The wind speed in the test section was calculated by the measurements of the dynamic pressure made through a Venturi system equipped with 4 static pressure probes located

at the side faces of the first and last section of the convergent segment of the tunnel. A pressure transducer with a 2500 Pa full-scale and a 3 Pa accuracy measured the static pressure variation between these sections, providing the dynamic pressure ahead of the test chamber. From the measurement of the dynamic pressure and the estimation of the air density by means of a temperature probe, the flow velocity in the test section was finally calculated. The angle of attack was measured with the mono-axial tilt sensor CrossBow CXTA01, which has an accuracy of 0.05° and a range from −75° to 75°. The sideslip angle was measured by a linear potentiometer whose installation provided an accuracy of 0.1° and a range from −15° to 25°.

The measurement of the aerodynamic forces and moments acting on the scaled model was made with internal strain gauge balances, mounted on a string also supporting the whole model, with the sensible part located within the fuselage. Two tri-axial balances—one measuring lift, drag, and pitching moment, the other measuring sideforce, yawing moment, and rolling moment—made of aluminium alloy 2024-T3 were used. Table 1 summarises the full-scale readings and the maximum errors per axis for the internal balances.

Table 1. Strain gauge balances characteristics.

Force/Moment	Max. Error	Full-Scale Value
Lift	0.03 kgf (0.06%)	80 kgf
Drag	0.02 kgf (0.10%)	20 kgf
Pitching moment	0.02 kgf m (0.10%)	20 kgf m
Side force	0.02 kgf (0.10%)	20 kgf
Yawing moment	0.02 kgf m (0.10%)	20 kgf m
Rolling moment	0.02 kgf m (0.10%)	20 kgf m

To evaluate the repeatability of the measurements and to quantify the spread in test data, in Table 2, the statistics concerning five tests on the same model configuration—Wing-Body (WB)—have been reported. Standard deviation (SD) values are shown for the lift, drag, and pitching moment coefficients. As concerns uncertainty in the yawing moment coefficient, data have been reported in Table 3 for the complete aircraft configuration, that is, Wing–Body–Horizontal–Vertical–Canard (WBHVC). Repeatability data for the load cells dedicated to the measurements of the propulsive forces are presented in Table 4.

Table 2. Uncertainty in measurements of lift, drag, and pitching moment coefficients. WB configuration. Test conditions: $V_\infty = 35\,\mathrm{m/s}$, Re = 315,000 at $\beta = 0°$.

α	C_L		C_D		C_M	
±0.1°	Mean	SD	Mean	SD	Mean	SD
−0.10	0.457	1.21%	0.0555	0.24%	−0.2079	0.58%
0.81	0.541	1.14%	0.0580	0.29%	−0.2052	0.62%
3.88	0.803	0.83%	0.0703	0.35%	−0.1857	0.53%
5.91	0.952	0.59%	0.0817	0.34%	−0.1636	0.50%

Table 3. Uncertainty in measurements of yawing moment coefficient. WBHVC configuration. Test conditions: $V_\infty = 35\,\mathrm{m/s}$, Re = 315,000 at $\alpha = 0°$.

β	C_N	
±0.1°	Mean	SD
0.0	−0.0023	0.05%
4.1	0.0067	0.08%
6.2	0.0114	0.08%
8.1	0.0152	0.08%
9.9	0.0175	0.10%

Table 4. Uncertainty in measurements of standalone propeller forces. Test conditions: $V_\infty = 35\,\mathrm{m/s}$, $\alpha = 4°$, $\beta = 0°$.

J	Axial Force, N		Normal Force, N	
±0.01	Mean	SD	Mean	SD
1.60	4.101	0.036	0.756	0.099
1.80	3.098	0.048	0.657	0.076
2.00	2.220	0.109	0.585	0.062
2.20	1.467	0.148	0.540	0.057
2.40	0.839	0.166	0.523	0.060
2.60	0.336	0.160	0.533	0.071
2.80	−0.041	0.133	0.571	0.091
3.00	−0.293	0.084	0.635	0.120

3. Propulsive Effects on the Horizontal Stabiliser

In this section, the key results concerning direct and indirect effects brought by the propeller slipstream on an innovative three-lifting surface high-capacity turboprop will be shown and discussed.

On a three-lifting surface aircraft, there is a strong coupling between the wakes and vortex systems coming from the wings. On the innovative configuration investigated in this work, this interaction is exacerbated by the reduced vertical stagger between the three wings. To minimise the effects of different wakes and their mutual interference on propulsive effects' measurement, the initial focus was on the configuration with the fuselage and empennage only. The effects of propeller rotation were also investigated.

3.1. Propulsive Effects on the BHV Configuration

The key objective of this research work is the assessment of the propeller slipstream impact on the aircraft's longitudinal static stability to ensure that non-detrimental effects are introduced by the rear-engine installation. Several tests have been fulfilled on the Body–Horizontal–Vertical tail (BHV) configuration to analyse the propulsive effects on the tailplane without any additional interference phenomena coming, especially from the canard. In this respect, the comparison has been carried out between a power-on condition and a configuration without propellers, but still with the supporting frame (power-off). Figure 10 shows the analysed configurations.

(**a**) (**b**)

Figure 10. Body-Horizontal-Vertical tail configuration tested in wind tunnel: (**a**) power-off BHV configuration; (**b**) power-on BHV configuration.

Scaled propeller data have been derived assuming reliable values for the full-scale engine thrust and rotational rate. Thrust similarity was achieved by matching the alternative thrust coefficient T_C [36]:

$$T_C = \frac{T}{\rho_\infty V_\infty^2 D^2} \quad (1)$$

where ρ_∞ is the air density, V_∞ is the airspeed, and D is the propeller diameter.

In Table 5, the scaled engine deck is summarised in terms of propeller coefficients, thrust, and power. The thrust coefficient T_C has already been defined above. The other variables are the standard Renard coefficients [37], rotational rate, thrust, and power. The selected operating points are representative of an average climb condition.

Table 5. Scaled engine deck for power-on wind tunnel tests—average climb conditions at 5000 ft.

J	C_T	C_P	η_p	T_C	RPM	T (N)	P (W)
1.46	0.59	1.13	0.77	0.28	9801	8.8	403
1.95	0.48	1.15	0.81	0.12	7351	4.0	174

However, during the tests, as with other similar experimental campaigns [22], it was found that the experimental apparatus was not able to provide the required power to reach the thrust corresponding to the most demanding operating points (9800 RPM). By the way, a meaningful value of T_C was still achieved, with a rotating speed about 1000 RPM lower than the target value, with an advance ratio J about 10% higher.

Two different propeller rotation directions were tested, see Figure 11. In the contra-rotating condition, both propellers rotate in the so-called Inboard-Up (IU) direction. In this condition, the inner tail sections impinged by the propeller slipstream will experience higher local induced angles in a symmetrical way, if no sidewash is present. Conversely, in the case of co-rotating propellers, the two horizontal stabilisers will experience an asymmetrical condition, in particular, the right half-tail will produce more lift than the left one.

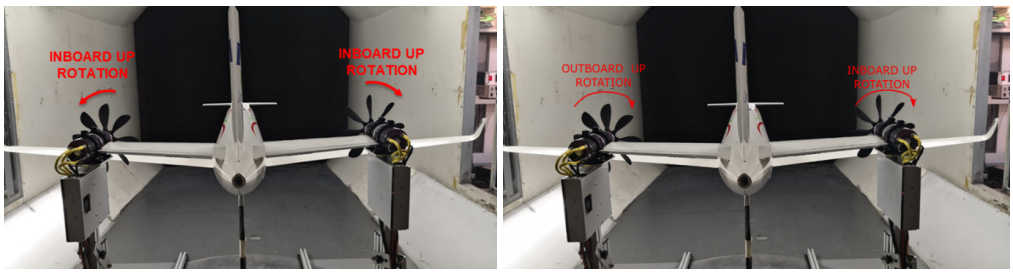

(**a**) (**b**)

Figure 11. Considered propeller rotation for the power-on experimental tests: (**a**) contra-rotating Inboard-Up (IU) propellers rotation; (**b**) co-rotating (CR) propellers rotation.

Figures 12 and 13 show the overall effects of the propulsion on the pitching moment and lift coefficient, respectively, for the contra-rotating (IU) propellers. In this case, the propulsion affected the longitudinal stability contribution of the tailplane as well as its lift capabilities. At the same angle of attack in the power-off condition, the tail was producing more lift because of the higher dynamic pressure brought by the propeller slipstream. The increased tail lift led to a greater negative pitching moment coefficient, which means greater longitudinal stability. The higher the RPM, the stronger the propeller blowing.

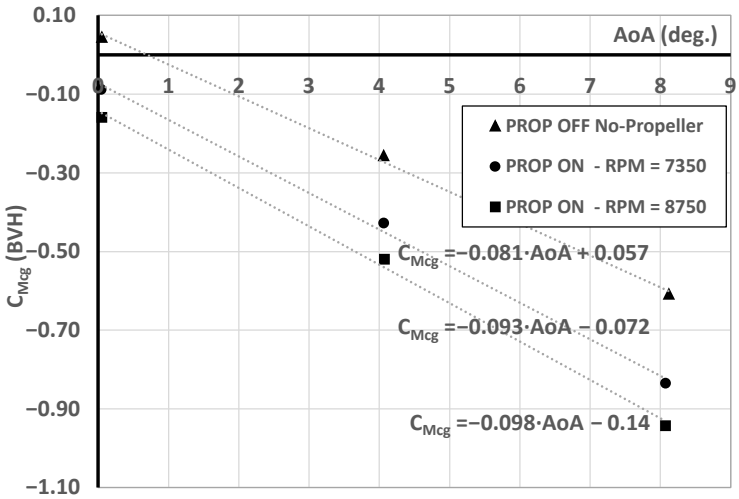

Figure 12. Global propulsive effects (direct and indirect) on the pitching moment coefficient curves for two engine design points and power-off conditions, Re = 315,000, X_{CG} at LE MAC, IU rotation at two RPM settings.

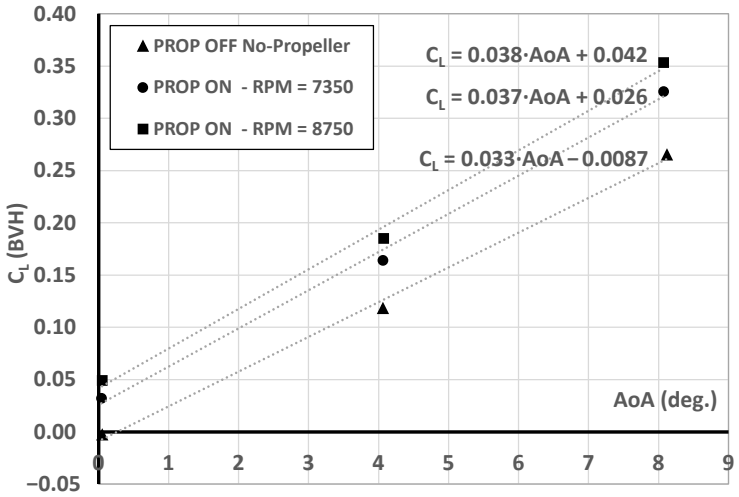

Figure 13. Global propulsive effects (direct and indirect) on the lift coefficient curves for two engine design points and power-off conditions, Re = 315,000, IU rotation at two RPM settings.

A summary of the overall propulsive effect on BHV lift and pitching moment coefficient slopes is provided in Table 6. Both the direct and indirect effect of the propulsion led to an increase in the lift curve slope, which was 14% higher with respect to the power-off condition, whereas the pitching moment slope was increased by 21% (considering the maximum achievable RPM = 8750).

Table 6. Global (direct and indirect) propulsive effects on lift and pitching moment coefficient curve slope, BHV aircraft configuration, Re = 315,000, CG at LE MAC.

Derivative (deg^{-1})	Power-Off	Power-On 7350 RPM	Power-On 8750 RPM	Δ Power-On/Off (w.r.t. 8750 RPM)
$C_{M_{\alpha_{BHV}}}$	−0.081	−0.093	−0.098	21%
$C_{L_{\alpha_{BHV}}}$	0.033	0.037	0.038	14%

However, as discussed in Section 1, the propulsive effects are the sum of the direct effects, measured by the load cells in the box under the electric motors and, therefore, decoupled from the wind tunnel balance, and the indirect effects, due to the local variation

of dynamic pressure and angle of attack, which were measured by the internal strain gauge balance. For the sake of clarity and scientific purposes, it is worth breaking down the overall propulsive effects between the direct and indirect effects.

Charts in Figures 14 and 15 illustrate the indirect effects of the propeller slipstream on the BHV lift and pitching moment coefficients, respectively. In these comparisons, none of the measured propeller forces (thrust and normal force) has been included in the calculation of the coefficients. Table 7 reports the numerical breakdown of the lift and pitching moment coefficients at different angles of attack.

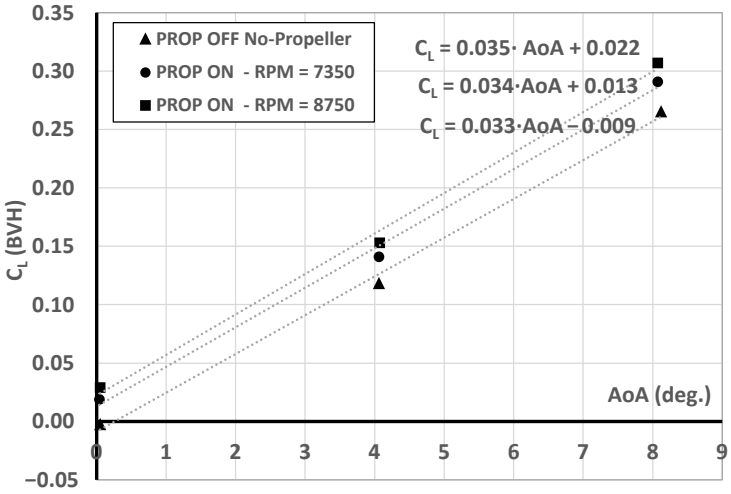

Figure 14. Indirect propulsive effect on the lift coefficient, *Re* = 315,000, IU rotation at two RPM settings.

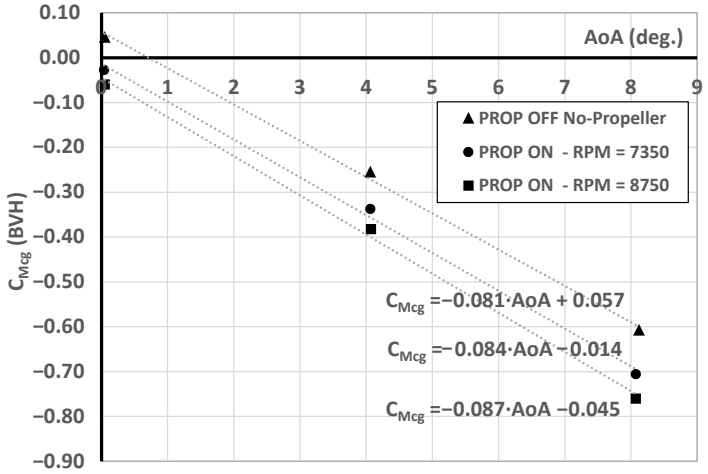

Figure 15. Indirect propulsive effect on the lift coefficient, *Re* = 315,000, X_{CG} at LE MAC, IU rotation at two RPM settings.

Table 7. Direct and indirect propeller effects breakdown, BHV aircraft configuration, *Re* = 315,000, X_{CG} at LE MAC, 8750 RPM (IU).

	Power-Off (No Propellers)		**Power-On (Indirect Effects)**		**Power-On (Overall Effects)**		**Propeller Forces (at 8750 RPM)**	
AoA (deg.)	C_L	$C_{M_{cg}}$	C_L	$C_{M_{cg}}$	C_L	$C_{M_{cg}}$	***T* (N)**	***N* (N)**
0.04	−0.003	0.045	0.029	−0.059	0.049	−0.159	3.908	1.213
4.06	0.118	−0.256	0.153	−0.382	0.185	−0.519	3.994	1.914
8.07	0.265	−0.608	0.307	−0.760	0.353	−0.942	4.128	2.768

Propeller disk is placed at X = 0.378 m and Z = 0.070 m from the LE of the MAC.

Table 8 provides for a clear split between direct and indirect effects. The indirect effects linked to the propeller slipstream provided for a lift curve slope increase of about 6% that, in turn, was almost linearly converted into tailplane contribution to aircraft longitudinal stability; in fact, the pitching moment coefficient slope increased by 7%. Most of the contribution to changes in the longitudinal stability was introduced by the direct propeller's contribution to the lift and pitching moment coefficient.

To sum up briefly, tests have confirmed the beneficial effect of the propulsion on longitudinal stability, with a 21% increase in the longitudinal stability derivative C_{M_α}.

Table 8. Breakdown of direct and indirect propulsive effects on lift and pitching moment coefficient curve slope, BHV aircraft configuration, experimental results, Re = 315,000, 8750 RPM (IU), X_{CG} at LE MAC.

Derivative (deg^{-1})	Power-Off	Indirect Effects	Direct + Indirect Effects
$C_{M_{\alpha_{BHV}}}$	−0.081	−0.087 (+7%)	−0.098 (+21%)
$C_{L_{\alpha_{BHV}}}$	0.033	0.035 (+6%)	0.038 (+14%)

3.2. Influence of Propeller Rotation Direction

As demonstrated by Dimchev [38] and by Van Arnhem et al. [21], the direction of propeller rotation may affect the tailplane aerodynamics due to a different induced angle distribution. An Outboard-Up (OU) rotation resolves into a lower value of lift force generated when compared with the case of an Inboard-Up (IU) rotation. In fact, for an IU rotation, the tip-mounted propeller introduces positive angles of attack on the tailplane, resulting in a higher lift coefficient on both tailplane semi-spans. Conversely, for an OU rotation, the induced angles of attack are negative. Alternatively, for the Co-Rotating (CR) case, a positive angle of attack is induced on the left half tailplane and a negative for the right half.

The available experimental set-up allowed for testing a different propeller rotation, in particular a Co-Rotating (CR) configuration, in which the right propeller has an Inboard-Up (IU) rotation, as is shown in Figure 11b.

Test results highlighted a difference of about 2% in the pitching moment coefficient of the BHV layout between the IU and CR configurations, whereas 1% was the difference between the lift curve slopes in IU and CR conditions, as reported in Table 9.

The observed behaviour is aligned with similar experimental investigations [21,38]. The overall effect on the global lift and pitching moment coefficient differs between the IU and the CR rotation because of the different distribution of the induced angles of attack on the two horizontal tailplane halves. In the case of CR rotation, the left half of the horizontal tailplane generates a weaker lift force with respect to the right one, and the total value is lower than the IU configuration. In the investigated case study, differences between the IU and CR rotation are quite low since the propellers have been specifically designed to match the thrust coefficient of a full-scale rotor, favouring the generation of an axial induction to replicate the swirl behind the propeller.

Table 9. Effect of propeller rotation on overall (direct + indirect) propulsive effects on lift and pitching moment coefficient curve slope, BHV aircraft configuration, experimental results, Re = 315,000, RPM 8750, X_{CG} at LE MAC.

Derivative (deg^{-1})	Power-Off	Power-On (IU)	Power-On (CR)
$C_{M_{\alpha_{BHV}}}$	−0.081	−0.098 (+21%)	−0.096 (+19%)
$C_{L_{\alpha_{BHV}}}$	0.033	0.038 (+14%)	0.037 (+13%)

4. Propulsive Effects on the Complete Aircraft Configuration

Both direct and indirect propeller effects were assessed in the previous section by investigating the BHV configuration minimising all potential interference with other aircraft

components. Co-rotating and contra-rotating propeller rotations were tested. The contra-rotating propellers were considered in order to magnify the slipstream effects by producing a symmetrical lift loading variation on both the horizontal tail semi-spans.

In general, co-rotating propellers are the most common scenario for real, full-scale aircraft. Counter-rotating propellers could balance the negative effects of torque and P-factor [31], meaning that a twin-engine aircraft would not have a critical engine in case of engine failure. Despite this advantage, to reverse the rotation of one propeller in a counter-rotating arrangement, there is the need for an additional reversing gearbox or the engines themselves must be adapted to run in opposite directions. The latter practically means having two engine designs, one with left-turning and the other with right-turning parts, which complicates manufacturing and increases maintenance costs.

In this section, the propulsive effects have been evaluated on the complete aircraft configuration, see Figure 16, assuming Co-Rotating (CR) propellers. Since propellers on most conventional twin-engine aircraft spin clockwise (as viewed from behind the engine), the assumed condition was exactly the one sketched in Figure 11b.

Figure 16. Aircraft complete configuration with electric motors.

4.1. Propulsive Effects on the Complete Aircraft Longitudinal Stability

The key objective of this section was the evaluation of the propeller slipstream impact on the longitudinal static stability of the complete aircraft. To this end, a restrained range of angles of attack going from −2 to 4 degrees has been investigated, being the typical range where the aerodynamic characteristics are supposed to be linear. Figure 17 show both direct and indirect effects in terms of lift curve, whereas the impact on the aircraft pitching moment is highlighted by the chart of Figure 18. As already shown by authors in [39], the canard wake was impinging the tailplane at low angles of attack, causing a large downwash and dynamic pressure loss. By increasing the angle of attack, the canard wake crossed the horizontal stabiliser, as highlighted by the simple flow visualisation illustrated in Figure 19. The addition of the third lifting surface—the canard— led to a non-linear behaviour of the pitching moment coefficient. As it can be appreciated in Figure 18, the pitching moment coefficient of the power-off condition was not linear over the entire range of investigated angles of attack. Thus, to minimise the non-linear effects due to the canard wake and its downwash on the tail aerodynamics, both the lift and the pitching moment coefficient slopes have been estimated in the range of angles of attack going from 2 to 4 degrees for both the power-off and power-on conditions. The breakdown between the indirect and overall propulsive effects is summarised in Table 10.

By looking at the derivatives of Table 10, in the complete aircraft configuration, the propulsive indirect effects affected the lift slightly more than the stability characteristic. It

is worth remarking that the measured forces and moments were made through a unique internal strain gauge balance; thus, the presented coefficients report the propulsive effects on the overall configuration's aerodynamics. Notwithstanding the higher increase in the lift than in the pitching moment, and considering the reduced stagger between the wing and the propellers, it was the authors' opinion that the propellers were also slightly altering the flow conditions on the wing.

Table 11 provides a breakdown of the direct and indirect effects on lift and pitching moment for all the tested angles of attack as well as the average measurements of the propeller forces. Referring to the chart of Figure 18, it is interesting to highlight that the propellers were reducing the non-linear effects by ingesting the wakes coming from the wing and from the canard. If, on the one hand, the latter was a beneficial effect, on the other, the propellers were working in a non-uniform flow.

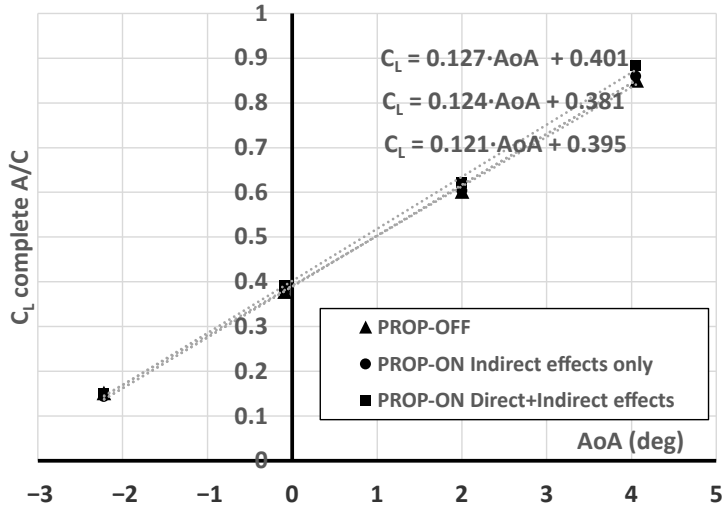

Figure 17. Indirect and direct propulsive effects on lift coefficient curves, experimental results, Re = 315,000, (CR) RPM 8750, X_{CG} at LE MAC.

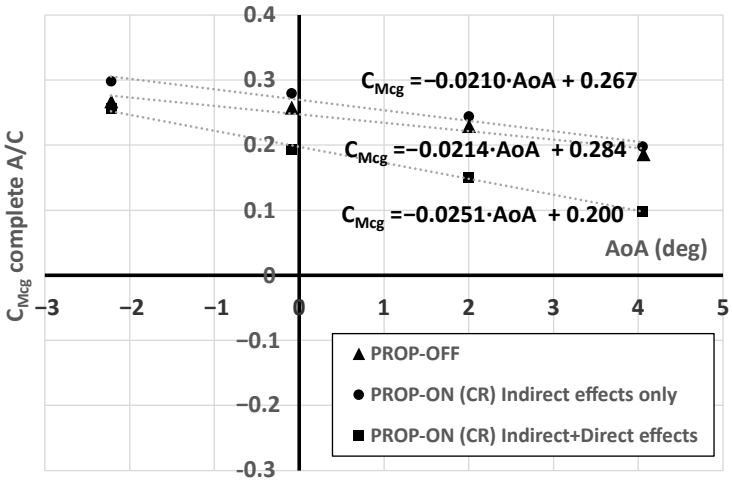

Figure 18. Indirect and direct propulsive effects on pitching coefficient curves versus α, experimental results, Re = 315,000, (CR) RPM 8750, X_{CG} at LE MAC.

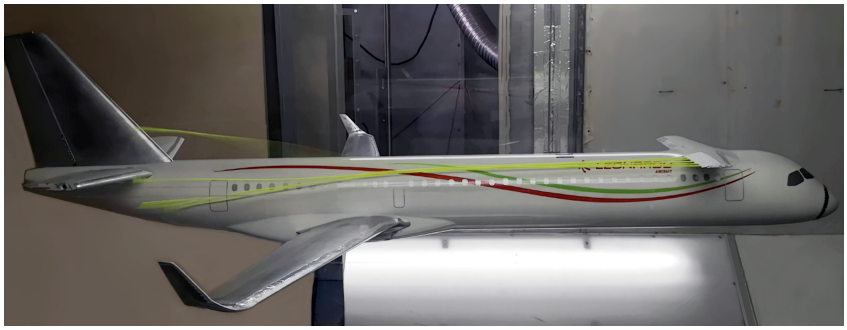

(**a**)

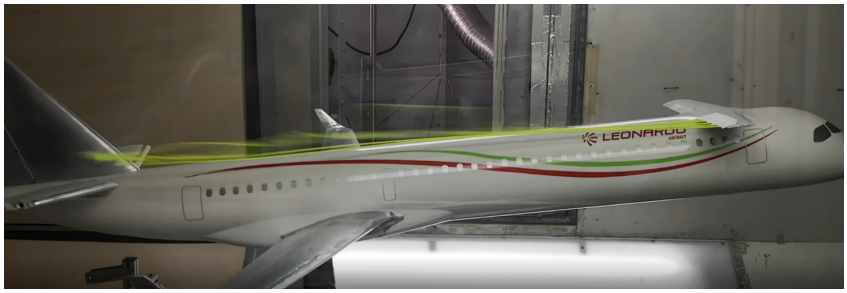

(**b**)

Figure 19. Displacement of the canard wake with respect to the horizontal tailplane: visualisation test through wool yarns: (**a**) $\alpha = 2°$; (**b**) $\alpha = 6°$.

Table 10. Breakdown of direct and indirect propulsive effects on lift and pitching moment coefficient curve slope, complete aircraft configuration, experimental results. Re = 315,000, RPM = 8750 (CR), X_{CG} at LE MAC.

Derivative (deg^{-1})	Power-Off	Indirect Effects	Direct + Indirect Effects
$C_{M_{\alpha_{AC}}}$	−0.0210	−0.0214 (+2%)	−0.0251 (+20%)
$C_{L_{\alpha_{AC}}}$	0.121	0.124 (+3%)	0.127 (+5%)

Considered range of angle of attack: 2–4 degrees.

Table 11. Direct and indirect propeller effects breakdown, on the complete aircraft configuration, Re = 315,000, X_{CG} at LE MAC, 8750 RPM (CR).

	Power-Off (No Propellers)		Power-On (Indirect Effects)		Power-On (Overall Effects)		Propeller Forces	
AoA (deg.)	C_L	$C_{M_{cg}}$	C_L	$C_{M_{cg}}$	C_L	$C_{M_{cg}}$	T (N)	N (N)
−2.22	0.152	0.267	0.144	0.2982	0.149	0.256	3.809	0.093
−0.09	0.378	0.258	0.376	0.2793	0.391	0.193	3.548	0.939
2.00	0.602	0.230	0.604	0.2441	0.622	0.150	3.525	1.118
4.05	0.850	0.186	0.859	0.1975	0.882	0.099	3.848	1.225

Propeller disk is placed at X = 0.378 m and Z = 0.070 m from the LE of the MAC.

Figure 20 shows a qualitative representation of the possible interference effects on the innovative aircraft configuration under investigation:

- asymmetric thrust distribution due to wing and canard wakes impinging the propellers' disks
- horizontal tailplane load varying with propeller load due to the flow swirl inducing vertical velocities at the tail
- different propellers thrust and normal force, even with identical propulsive units, due to the above-mentioned aerodynamic effects.

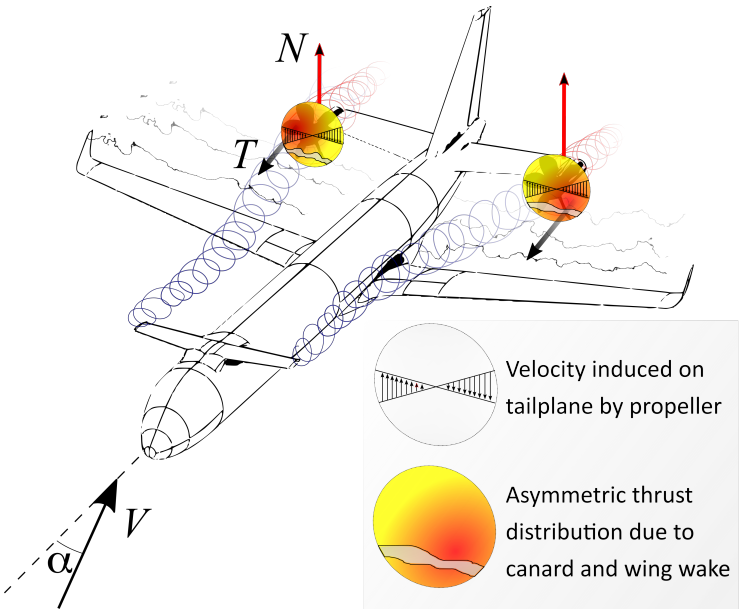

Figure 20. A qualitative sketch of aero-propulsive interactions on the IRON innovative aircraft.

The detrimental effects on the propeller's performance due to the aforementioned effects are clearly outlined by the comparison of the propeller forces shown in Table 11, in the case of the complete aircraft configuration, with the values reported in Table 7 for the BHV configuration. An average loss of about 7% in thrust has been estimated, whereas the average normal force is reduced by 59%. The latter highlights how the flow field investing the propellers disk was affected by the downwash from the wing and especially from the canard. This downwash reduces the net incidence angles at the propeller disks, letting the propellers work in an almost axial flow condition.

4.2. Propulsive Effects on Complete Aircraft Lateral-Directional Stability

Several tests have been also performed to investigate the propulsive effects on lateral and directional stability on the complete aircraft configuration. In this respect, the yawing moment coefficient, C_N, and the rolling moment coefficient, $C_{\mathcal{L}}$, are defined as the moment around the vertical (Z-axis) and the longitudinal (X-axis) of a reference system having its origin in the aircraft centre of gravity. The aim of these experimental tests was to estimate the stability derivatives, C_{N_β} and $C_{\mathcal{L}_\beta}$, quantifying the effect the propulsion has on these aerodynamic characteristics. Regarding the power-on conditions, the Co-Rotating (CR) propellers were still considered power-on conditions. It is worth highlighting that the available measurement system for this experimental investigation was not capable of measuring any side force (C_{Y_p}) produced by the propellers. Thus, concerning directional and lateral stability characteristics, the direct propeller effects could not be assessed. However, the performed experimental tests still provided some interesting scientific results concerning the propeller slipstream effects on the aircraft's lateral and directional stability characteristics.

The first effect that could be highlighted dealt with the aircraft rolling moment coefficient. Referring to the chart of Figure 21, it is possible to appreciate that the rolling moment derivative was increased in the power-on conditions. In the considered power-on tests, the right propeller was spinning in an Inboard-Up rotation, whereas the left propeller had an Outboard-Up rotation, the different rotating directions caused a lift imbalance between the right and the left tail semi-spans. In fact, the right tail region affected by the propeller slipstream was experiencing higher angles of attack, on the contrary, the same tail portion on the left tail span was affected by a local incidence angle reduction. Since the tailplane at low angles of attack was producing a downforce due to the downwash from the wing and canard, the right tail was producing a lower downforce than the left one, with a consequent increase in the aircraft rolling moment slope with respect to the sideslip angle.

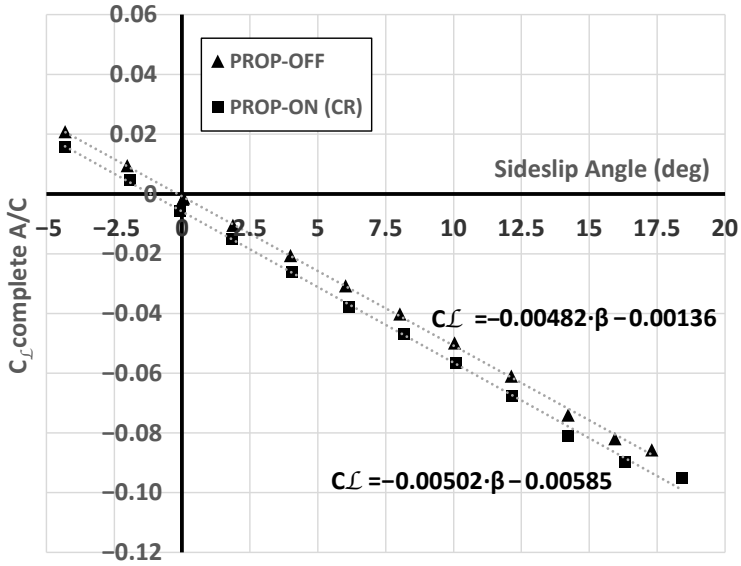

Figure 21. Indirect propeller slipstream effects on complete aircraft rolling moment coefficient, experimental results, Re = 315,000, 8750 RPM (CR), X_{CG} at LE MAC, α = 0 deg.

This aerodynamic behavior is qualitatively explained in the chart of Figure 22.

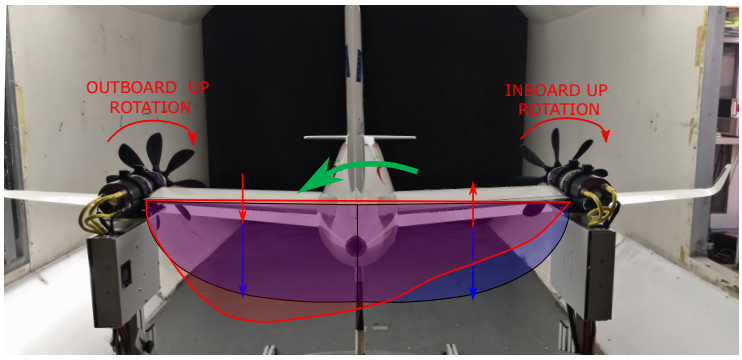

Figure 22. Qualitative explanation of induced rolling moment due to propulsive effects (Co-Rotating propellers). Due to the propellers rotation, the tail lift distribution and the resultant lift force are modified. The blue curve and arrows are representative of the lift distribution and resultant force in in prop-off condition, whereas the red curve and arrows are representative of the prop-on condition. The green arrow indicates the direction of the resulting rolling moment in prop-on condition.

The other aerodynamic characteristic to be investigated was the yawing moment coefficient C_N and its derivative with respect to the sideslip angles C_{N_β}. The chart of Figure 23 shows the comparison between the power-on and the power-off yawing moment coefficient variation with respect to the sideslip angle. The first aspect that must be here highlighted is that the directional stability of the complete aircraft exhibits a nonlinear behaviour in a specific sideslip angle range in both power-off and power-on conditions.

This nonlinear yawing moment variation was, once again, due to the canard wake. In this particular case, this effect was introduced by the canard tip vortex system, which was impinging the vertical empennage. As shown by a simple visualization test made through the application of wool yarns on the canard trailing edge (see Figure 24), the canard tip vortex system at low sideslip angles was impinging the windward side of the vertical tail, reducing its capability to produce sideforce. As the sideslip angle increases, the tip vortex moves across the vertical tail; when it reaches the leeward side of the empennage, the lifting capabilities of the tail are suddenly recovered. This latter effect occurs at sideslip angles higher than 10 degrees, as it can be appreciated in the charts of Figure 23.

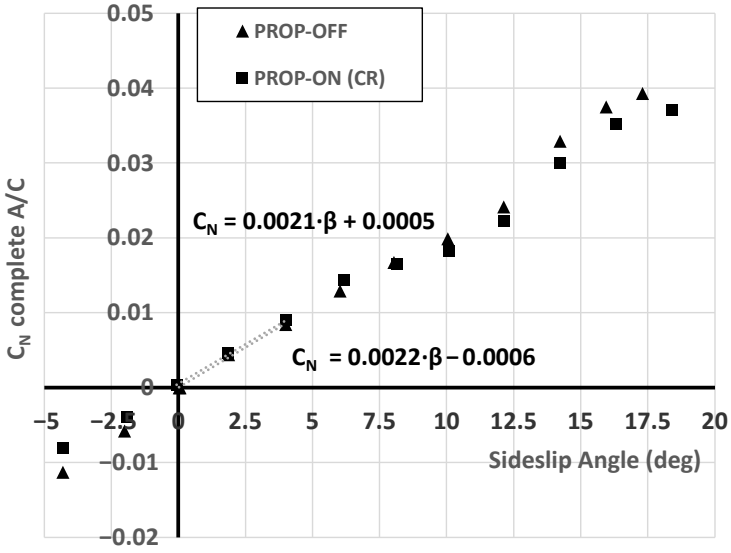

Figure 23. Indirect propeller slipstream effects on complete aircraft yawing moment coefficient, experimental results (Re = 315,000, 8750 RPM (CR), X_{CG} at LE MAC), α = 0 deg.

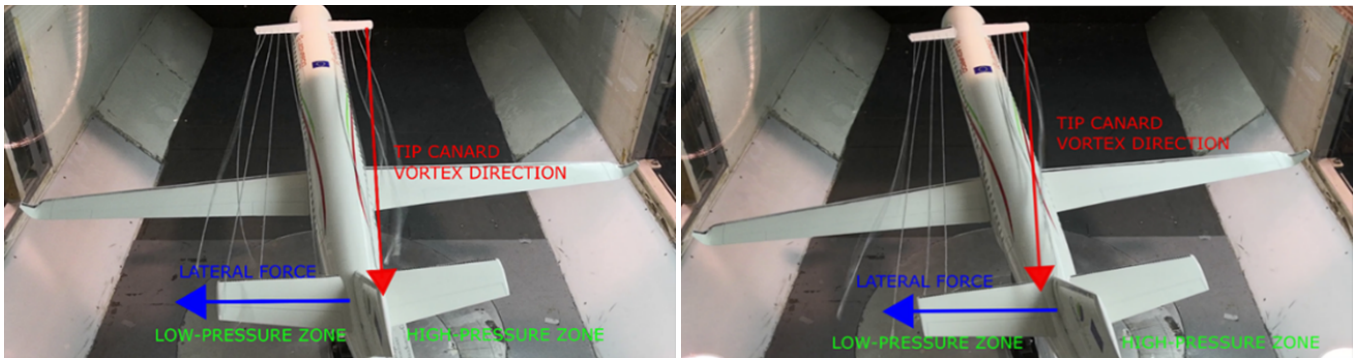

(**a**) (**b**)

Figure 24. Simple canard wake visualisation through wool yarns stitched to the canard trailing edge: (**a**) β = 8 deg; (**b**) β = 10 deg.

A similar phenomenon has also been observed by Agnew et al. in [40] for a three-surface fighter aircraft. The physical behaviour was similar, notwithstanding the clear differences in the aircraft configurations. Notwithstanding the aforementioned nonlinear phenomena, to minimise the impact these effects have on the estimate of the yawing moment derivative, a range of sidelip angles from zero up to four degrees has been identified as the most suitable range in which to perform the derivative estimation. A summary of the indirect propulsive effects is shown in Table 12, where in the considered range of sideslip angles, both the rolling and the yawing moment coefficient derivatives are compared in power-off and power-on conditions.

Table 12. Indirect propulsive effects on directional and lateral stability derivatives, experimental results (Re = 315,000, V = 35 m/s, 8750 RPM (CR), X_{CG} @LE MAC), α = 0 deg.

	Power-Off	**Power-On CR**
C_{N_β} deg^{-1}	0.0022	0.0021 (−4%)
$C_{\mathcal{L}_\beta}$ deg^{-1}	−0.0048	−0.0050 (+4%)

In contrast with the outcomes of Perkins [31] and Van Arnhem et al. [21], the estimated directional stability of the aircraft was slightly affected by the propulsion (Figure 23): the

stability derivative C_{N_β} is even lower for the power-on conditions, as reported in Table 12. However, the configurations investigated by Perkins [31] and Van Arnhem et al. [21] provided for engine installation in different positions with respect to the one considered for this work (wing-mounted and on the middle of the tailplane, respectively). Probably, for the configuration investigated in this work, the reduction of yawing moment coefficient in power-on conditions was the result of different interference phenomena due to propeller installation and rotating direction. Since, in this particular layout, engines were placed at the tail tips quite far from the vertical empennage, the propeller's slipstream did not strongly impact the vertical fin like the case of a wing or mid-tail mounted engines. Notwithstanding the positioning and the assumed rotating directions, propellers affected the horizontal tail drag more, as a consequence of the changes in the lift distribution, rather than of the pressure field between the two sides of the vertical fin, to generate more sideforce.

5. Conclusions

This paper investigated how the propulsive system affected the horizontal tailplane aerodynamics and, consequently, the aircraft static stability of a three-lifting surface turboprop aircraft concept, with rear engines installed at the horizontal tail tips. Both direct and indirect propulsive effects were assessed by means of a wind tunnel test carried out at the main low-speed facility of the University of Naples "Federico II".

Firstly, several tests were performed on the body-empennage configuration to investigate the propulsive effects on the horizontal stabilisers, minimising any aerodynamic interference phenomena coming especially from the canard. At the same flow condition of the power-off test, the tail produced more lift thanks to the higher dynamic pressure brought by the propeller slipstream. The increased tail lift led to a greater negative pitching moment coefficient, with a consequently higher longitudinal stabilizing effect. This increment has been estimated equal to 21% in terms of the pitching moment coefficient derivative with respect to the angle of attack. Additionally, for this kind of configuration, the propeller rotation direction effect, co-rotating and counter-rotating inboard-up, was investigated. It was found that in the case of co-rotating direction, the gain in terms of the pitching moment coefficient was slightly lower than the inboard-up rotation (+19% instead of +21%). The main reason for this difference lay behind the different distribution of the induced angles of attack on the two horizontal tailplane halves: in the case of co-rotating rotation, the left half of the horizontal tailplane generated a weaker lift force with respect to the right one, and the total value was lower than the inboard-up configuration.

Then, the propeller slipstream impact on the longitudinal static stability of the complete aircraft was evaluated. To this end, the typical range in which the aerodynamic characteristics were supposed to be linear was investigated. However, to minimise the nonlinear effects due to the canard wake and its downwash on the tail aerodynamics, the slope derivatives for both the lift and the pitching moment coefficient were estimated in the range of angles of attack from two up to four degrees for both the power-off and power-on conditions.

The output of the experimental campaign on the complete aircraft, confirmed the beneficial effect of the propulsive effects on the aircraft's longitudinal stability, with an increase of 21% in terms of the pitching moment coefficient (which corresponds to a higher stability margin of about 2.5%), and a 5% higher lift coefficient derivative.

Finally, several tests were also performed to investigate the propulsive effects on lateral and directional stability of the complete aircraft configuration. Concerning the lateral stability, the rolling moment derivative was 4% higher in the power-on conditions due to different rotating directions, which caused a lift imbalance between the right and the left tail semi-spans (it is important to remember that the investigated direction for complete aircraft was the co-rotating one, which means that the right propeller spun in an inboard-up direction, whereas the left propeller spun in outboard-up direction).

As for the longitudinal case, the directional stability analysis was also affected by the nonlinear effects due to the canard tip wake and its sidewash on the vertical tail

aerodynamics. In fact, the canard tip vortex system at low sideslip angles impinged on the windward side of the vertical tail, reducing its capability to produce sideforce. As the sideslip angle increased, the tip vortex moved across the vertical tail, when it reached the leeward side of the empennage, the lifting capabilities of the tail were suddenly recovered. For this reason, a range of sidelip angles from 0 up to 4 degrees has been considered to perform the derivative estimation. Regarding directional stability, a reduction in the yawing moment coefficient derivative of about 4% was observed, which could be attributed to the different drag contributions of the two horizontal tail semi-planes. Probably, this reduction was due to the propeller installation and rotating direction. Indeed, since in this particular layout, engines were placed at the tail tips quite far from the vertical empennage, the propeller's slipstream did not strongly impact the vertical fin as in the case of wing- or mid-tail-mounted engines, but they affected the horizontal tail drag more than the pressure field between the two sides of the vertical fin to generate more side-force.

The authors would like to conclude by saying that the intention of this research was to perform design activities concerning an innovative regional turboprop. In this respect, this work is a part of that research, and it represents an important step towards the demonstration of the technical feasibility of such an innovative configuration. In particular, the outcomes of this paper allow for the enhancement of the technical readiness level of the considered aircraft, giving clear indications on several aspects concerning propulsive effects and their interaction with the interference effects among the lifting surfaces already investigated in the previous work.

Author Contributions: Conceptualisation, S.C. and V.C.; methodology, S.C. and V.C.; experimental setup, S.C., D.C. and V.C.; tests, V.C. and S.C.; resources, F.N.; data curation, S.C. and V.C.; writing—original draft preparation, S.C., V.C. and D.C.; writing and editing, S.C., V.C. and D.C.; review V.C., S.C. and D.C.; visualization, S.C., V.C. and D.C.; supervision, F.N. All authors have read and agreed to the published version of the manuscript.

Funding: The IRON project has received funding from the Clean Sky 2 Joint Undertaking under the European Union Horizon 2020 research and innovation program under Grant Agreement no. 807089.

Institutional Review Board Statement: Not applicable.

Informed Consent Statement: Not applicable.

Data Availability Statement: The authors confirm that the data supporting the findings of this study are available within the article.

Acknowledgments: The authors are grateful to the partners of the IRON consortium for their contributions and feedback.

Conflicts of Interest: The authors declare no conflict of interest. The funders had no role in the design of the study; in the collection, analyses, or interpretation of data; in the writing of the manuscript; or in the decision to publish the results.

Abbreviations

The following abbreviations and symbols are used in this manuscript:

AC	Complete aircraft configuration
AoA	Angle of Attack
$C_{(\cdot)_\alpha}$	Derivative of the aerodynamic coefficient with respect to α
$C_{(\cdot)_\beta}$	Derivative of the aerodynamic coefficient with respect to β
CG	Center of Gravity
C_L	Lift coefficient
$C_{\mathcal{L}}$	Rolling moment coefficient
C_M	Pitching moment coefficient with respect of the centre of gravity
C_N	Yawing moment coefficient
CNC	Computer Numerical Control
C_P	Propeller power coefficient
C_Q	Propeller torque coefficient

CR	Co-Rotating
C_T	Propeller thrust coefficient
C_{Y_P}	Propeller sideforce coefficient
ESC	Electronic Speed Controller
IRON	Innovative turboprop configuration
IU	Inboard-Up rotation
J	Advance ratio
LE	Leading Edge
MAC	Mean Aerodynamic Chord
N	Propeller normal force
OU	Outboard Up rotation
P	Power absorbed by electric motors
Re	Reynolds number
RPM	Round per minutes
T	Propeller thrust force
T_C	Propeller alternative thrust coefficient
TSA	Three lifting Surface Aircraft
V_∞	Wind tunnel flow speed
X_{CG}	Longitudinal position of the CG in fraction of MAC
α	Angle of Attack
β	Angle of sideslip
η_P	Propeller efficiency

References

1. Liebeck, R.; Page, M.; Rawdon, B. Blended-Wing-Body Subsonic Commercial Transport. In Proceedings of the 36th AIAA Aero-space Sciences Meeting and Exhibition, Reno, NV, USA, 12–15 January 1998. [CrossRef]
2. Okonkwo, P.; Smith, H. Review of evolving trends in blended wing body aircraft design. *Prog. Aerosp. Sci.* **2016**, *82*, 1–23. [CrossRef]
3. Schiktanz, D.; Scholz, D. Box Wing Fundamentals—An Aircraft Design Perspective. Deutsche Gesellschaft für Luft- und Raumfahrt. 2011. ISBN 978-3-932182-74-X. Available online: https://web.archive.org/web/20220929021705fw_/https://www.fzt.haw-hamburg.de/pers/Scholz/Airport2030/Airport2030_ART_BoxWingAircraft_13-06-05.pdf (accessed on 2 October 2022).
4. Jemitola, P.; Fielding, J. Box Wing Aircaft Conceptual Design. In Proceedings of the 8th International Congress of the Aeronautical Sciences, Brisbane, Australia, 2–4 July 2012.
5. Cipolla, V.; Frediani, A.; Abu Salem, K.; Picchi Scardaoni, M.; Nuti, A. Conceptual design of a box-wing aircraft for the air transport of the future. In Proceedings of the Aviation Technology, Integration, and Operations Conference, Indianapolis, IN, USA, 17–19 September 2012. [CrossRef]
6. Strohmeyer, D.; Seubert, R. Three Surface Aircraft—A concept for future transport aircraft. In Proceedings of the 38th AIAA Aerospace Sciences Meeting and Exhibition, Reno, NV, USA, 10–13 January 2000. [CrossRef]
7. Wichmann, G.; Strohmeyer, D.; Streit, T. Three-Surface aircraft—A Concept for Future large aircraft. In Proceedings of the 22nd International Congress of Aeronautical Sciences, Dubai, United Arab Emirates, 18–20 November 2012.
8. Nicolosi, F.; Corcione, S.; Della Vecchia, P.; Trifari, V.; Ruocco, M. Aerodynamic design and analysis of an innovative regional turboprop configuration. In Proceedings of the 31st ICAS Conference (International Council of the Aeronautical Sciences, Belo Horizonte, Brazil, 9–14 September 2018.
9. Goetzendorf-Grabowski, T.; Antoniewski, T. Three surface aircraft (TSA) configuration—Flying qualities evaluation. *Aircr. Eng. Aerosp. Technol.* **2016**, *88*, 277–284. [CrossRef]
10. Cacciola, S.; Riboldi, C.; Arnoldi, M. Three-Surface Model with Redundant Longitudinal Control: Modeling, Trim Optimization and Control in a Preliminary Design Perspective. *Aircr. Eng. Aerosp. Technol.* **2016**, *8*, 139. . [CrossRef]
11. Selberg, B.; Rokhsaz, K. Aerodynamic tradeoff study of conventional, canard, and trisurface aircraft systems. *J. Aircr.* **1985**, *23*, 768–774. [CrossRef]
12. Ostowari, C.; Naik, D. Experimental study of three-lifting surface configuration. *J. Aircr.* **1985**, *25*, 106–112. [CrossRef]
13. Patek, Z.; Smrcek, L. Aerodynamic characteristics of multi-surface aircraft configurations. *Aircr. Des.* **1999**, *2*, 191–206. [CrossRef]
14. Owens, D.; Perkins, J. Stability and control of a three-surface, forward-swept wing configuration. *J. Aircr.* **2012**, *33*, 191–206. [CrossRef]
15. Nicolosi, F.; Corcione, S.; Trifari, V.; De Marco, A. Design and Optimization of a Large Turboprop Aircraft. *Aerospace* **2021**, *8*, 132. [CrossRef]
16. Goldsmith, I.M. *A Study to Define the Research and Technology Requirements for Advanced Turbo/Propfan Transport Aircraft*; Technical Report; Report Number NASA-CR-166138; McDonnell Douglas Corporation: Washington, DC, USA, 1981. Available online: https://ntrs.nasa.gov/citations/19820010328 (accessed on 15 December 2023).

17. Veldhuis, L.L.M. Review of Propeller-Wing Aerodynamic Interference. In Proceedings of the 24th Congress of the International Council of Aeronautical Science, Yokohama, Japan, 29 August–3 September 2004.
18. Obert, E. The Effect of Propeller Slipstream on the Static Longitudinal Stability and Control of Multi-Engined Propeller Aircraft. In Proceedings of the 19th Congress of the International Council of Aeronautical Sciences, Anaheim, CA, USA, 18–23 September 1994.
19. Bouquet, T.; Vos, R. Modeling the propeller Slipstream Effect on Lift and Pitching moment. In Proceedings of the 2017 AIAA Aerospace Sciences Meeting, Grapevine, TX, USA, 9–13 January 2017. [CrossRef]
20. van Arnhem, N.; Sinnige, T.; Stokkermans, T.; Eitelberg, G.; Veldhuis, L. Aerodynamic Interaction Effects of Tip-Mounted Propellers Installed on the Horizontal Tailplane. In Proceedings of the 2018 AIAA Aerospace Sciences Meeting, Kissimmee, FL, USA, 8–12 January 2018. [CrossRef]
21. van Arnhem, N.; De Vries, R.; Vos, R.; Veldhuis, L.M. Aerodynamic Performance of an Aircraft Equipped with Horizontal Tail Mounted Propellers, In Proceedings of the AIAA Aviation 2019 Forum, Dallas, TX, USA, 17–21 June 2019. [CrossRef]
22. van Arnhem, N.; de Vries, R.; Sinnige, T.; Vos, R.; Veldhuis, L. Aerodynamic Performance and Static Stability Characteristics of Aircraft with Tail-Mounted Propellers. *J. Aircr.* **2022**, *59*, 415–432. [CrossRef]
23. Obert, E. *Aerodynamic Design of Transport Aircraft* ; IOS Press: Delft, The Netherlands; 2009. ISBN 978-1-58603-970-7.
24. Witkowsky, D.; Lee, A.; Sullivan, J. Aerodynamic Interaction Between for Propellers and Wings. *J. Aircr.* **1989**, *26*, 829–836. [CrossRef]
25. Witkowsky, D.; Johnston, R.; Sullivan, J. Propellers/Wing Interaction. In Proceedings of the AIAA 27th Aerospace Sciences Meeting, Reno, NV, USA, 9–12 January 1989. [CrossRef]
26. Veldhuis, L. Propeller Wing Aerodynamic Interference. Ph.D. Thesis, Delft University of Technology, Delft, The Netherlands, 2005.
27. Miranda, L.; Brennan, J. Aerodynamic Effects of Wing-Mounted Propellers and Turbines. In Proceedings of the AIAA 4th Applied Aerodynamics Conference, San Diego, CA, USA, 9–11 June 1986. [CrossRef]
28. Kroo, I. Propeller/wing integration for minimum induced loss. *J. Aircr.* **1986**, *23*, 561–565. [CrossRef]
29. van de Borne, P.; van Hengst, J. Investigation of propeller slipstream effects on the Fokker 50 through in flight pressure measurements. In Proceedings of the Flight Simulation Technologies Conference and Exhibit, Dayton, OH, USA, 17–19 September 1990.
30. Schroijen, M.; Slingerland, R. Propeller Slipstream Effects on Directional Aircraft Control with One Engine Inoperative. In Proceedings of the 45th AIAA Aerospace Sciences Meeting and Exhibit, Reno, NV, USA, 8–11 January 2007. [CrossRef]
31. Perkins, C.D.; Hage, R.E. *Airplane Performance Stability and Control*; Wiley: New York, NY, USA, 1949; p. 502.
32. Ribner, H.S. *Propellers in Yaw*; Technical Report; NACA: Washington, DC, USA, 1943.
33. De Young, J. Propeller at high incidence. *J. Aircr.* **1965**, *2*, 241–250. [CrossRef]
34. Nicolosi, F.; Corcione, S.; Della Vecchia, P.; Trifari, V.; Ruocco, M.; De Marco, A. Design and aerodynamic analysis of a regional turboprop innovative configuration. In Proceedings of the 6th CEAS Air and Space Conference (CEAS 2017), Bucharest, Romania, 16–20 October 2017.
35. Nicolosi, F.; Corcione, S.; Trifari, V.; Della Vecchia, P.; De Marco, A. Design Guidelines for High Capacity Innovative Regional Turboprop Aircraft. In Proceedings of the AIAA Scitech 2019 Forum, San Diego, CA, USA, 7–11 January 2019. [CrossRef]
36. Barlow, J.B.; Rae, W.H.; Pope, A. *Low-Speed Wind Tunnel Testing*, 3rd ed.; Wiley: New York, NY, USA, 1999.
37. Ciliberti, D.; Nicolosi, F. Design, Analysis, and Testing of a Scaled Propeller for an Innovative Regional Turboprop Aircraft. *Aerospace* **2022**, *9*, 264. [CrossRef]
38. Dimchev, M. Experimental and Numerical Study on Wingtip Mounted Propellers for Low Aspect Ratio UAV Design. Master's Thesis, Delft University of Technology, Delft, The Netherlands, 2012.
39. Cusati, V.; Corcione, S.; Ciliberti, D.; Nicolosi, F. Design Evolution and Wind Tunnel Tests of a Three-Lifting Surface Regional Transport Aircraft. *Aerospace* **2022**, *9*, 133. [CrossRef]
40. Agnew, J.; Lyerla, G.; Grafton, S. Linear and Nonlinear Aerodynamics of Three-Surface Aircraft Concepts. *J. Aircr.* **2012**, *18*, 956–962. [CrossRef]